Automated three-dimensional reconstruction of the *Caenorhabditis elegans* germline

Sandeep Gopal[a,b,*], Peter Boag[a,c], Roger Pocock[a,b,*]

[a] Development and Stem Cells Program, Monash Biomedicine Discovery Institute, Australia
[b] Department of Anatomy and Developmental Biology, Monash University, Melbourne, Victoria 3800, Australia
[c] Department of Biochemistry and Molecular Biology, Monash University, Melbourne, Victoria 3800, Australia

A R T I C L E   I N F O

A B S T R A C T

The *Caenorhabditis elegans* germline is widely used as a model to study stem cell development, chromosome dynamics and apoptosis. Major readouts of germline phenotypes such as cell counting and protein expression profiling are routinely analyzed manually and in a two-dimensional manner. The major disadvantages of the existing approaches are 1) they are time-consuming and laborious and 2) there is an inability to study the effects of genetic mutations in three dimensions. Here, we demonstrate a rapid, automated method for analyzing the three-dimensional distribution of proteins, germline nuclei and cytoskeletal structures in the *C. elegans* germline. Using this method, we have revealed previously unappreciated germline organization and cytoskeletal structures that will have a major impact on the characterization of germline phenotypes. To conclude, our new method dramatically enhances the efficiency and resolution of *C. elegans* germline analysis and may be applied to other cellular structures.

1. Introduction

The germline of *C. elegans* is extensively used to study molecular mechanisms that control stem cell development, gene regulation and apoptosis (Hubbard, 2007; Salinas et al., 2006). This is largely due to considerable conservation with mammalian signaling pathways and the presence of a well-defined stem cell niche (Hubbard, 2007; Joshi et al., 2010). Despite of its importance, the *C. elegans* germline is largely examined in two dimensions, somewhat limiting research potential. The *C. elegans* adult hermaphrodite germline has two independent arms within which germ cells develop in an assembly-line fashion. At the distal end of each germline arm is the somatic distal tip cell (DTC) which signals to maintain adjacent germ cells in an undifferentiated state (Byrd et al., 2014; Hubbard, 2007). As germ cells migrate proximally, the DTC signal is lost and germ cells enter meiotic prophase I in the transition zone (Kershner et al., 2013). These meiotic nuclei finally differentiate into sperm during the fourth larval stage and then oocytes in the adult stage.

The effect of DTC signals and differentiation drivers on germ cells is studied by analyzing nuclear proliferation, differentiation and apoptosis (Berry et al., 1997; Schumacher et al., 2005). This requires quantification of nuclei number, and the identification of initial differentiation points by observing changes in nuclear morphology,

chromosomal organization and expression of molecular markers. Manual cell counting and phenotypic analysis based on protein expression is time-consuming, labor-intensive and subject to human error. To circumvent these shortcomings, we developed an automated method not only for germline cell counting, but also for examining the distribution of nuclei and germline proteins (Fig. 1 **and** Box 1**)**. Further, two-dimensional analysis is unlikely to fully represent in vivo germline events. Therefore, we performed three-dimensional germline analysis to fully understand nuclear and protein dynamics. Our analysis also examined structural features of the germline cytoskeleton at different regions of the germline. This analysis has revealed previously unappreciated germline cytoskeletal structures, which we propose are of functional importance for germline development. These discoveries have been made possible by using confocal microscopy combined with advanced tools for three-dimensional rendering.

2. Results and discussion

Two-dimensional analysis of DAPI-stained wild type hermaphrodite germlines shows that the mitotic region and transition zone are approximately 21 and 11 nuclei in length, respectively (mitotic zone = 20.21 ± 0.25, transition zone = 10.69 ± 0.395, n > 30) (Fig. 2**a**). We used Imaris 8.4.1 rendering software to convert confocal micrographs

---

* Corresponding authors at: Development and Stem Cells Program, Monash Biomedicine Discovery Institute, Australia.
E-mail addresses: sandeep.gopal@monash.edu (S. Gopal), roger.pocock@monash.edu (R. Pocock).

of germlines into 3D dimensional surfaces and spots (Figs. 1, 2 **and** Box 1**)**. This MATLAB compatible software can develop intensity specific images after subtracting background, calculate distance between staining intensity centers and 3D interpret microscopy data sets. Our three-dimensional rendering of the *C. elegans* germline assigns specific shapes for mitotic, transition zone and meiotic nuclei, as previously described (Hirsh et al., 1976). In the mitotic and meiotic regions, nuclear morphology appears globular, whereas in the transition zone nuclear morphology appears oval in the Z-axis (Fig. 2**b and f**). For nuclear counting, each DAPI-stained nucleus is identified as a

spot in the germline (Fig. 2**c**). The correct assignment of cell size is crucial for accurately counting cell number and mapping cell distribution. For calculation of total nuclei number, the XY nuclear diameter is defined as 2 µm (discounting the Z diameter). Increasing the diameter to 2.5 µm accounts for larger late pachytene nuclei, whereas for the transition zone, a Z diameter of 1.5 µm may be applied to account for the different nuclear morphology. Multiple hermaphrodite germlines from young adult wild type animals (n =15) were quantified instantaneously using this method (compared to > 1 h of manual counting per germline) and the resultant data (total = ~1200 nuclei, mitotic region =
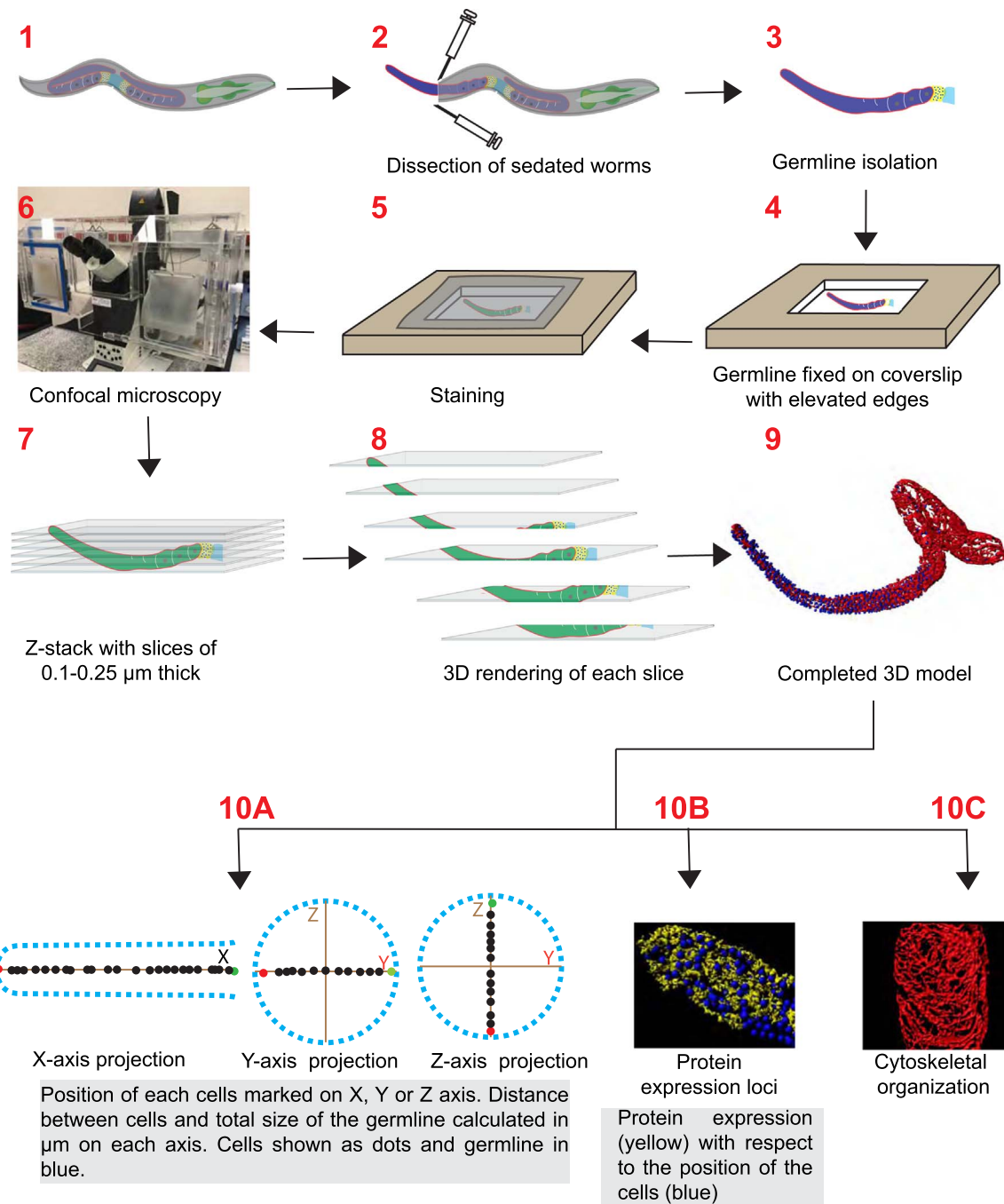

Fig. 1. Procedure for 3D modeling of the *C. elegans* germline Step 1–3: Young adult worms are sedated with 0.01% tetramisole and germlines dissected. Dissection at the uterus enabled complete germline isolation. Step 4: Place and fix dissected germlines on poly-L-lysine coated slide with elevated edges. Step 5: Apply appropriate antibodies or dyes for germline staining. A coverslip is placed on the slides covering the germlines (high edges to avoid crushing the germlines). Step 6–7: Stained germlines are imaged using confocal microscopy and slices of 0.1–0.5 µm thick are generated. Step 8–9: Each slice is developed into the 2D model before combining them into the complete 3D model. Step 10A-C: The 3D models can be used to study nuclear distribution within the germline by projecting the position of nuclei into X, Y and Z axes. In addition to the nuclear position, the total number of nuclei in each region will be automatically calculated accounting for changes in nuclei size and shape in each germline region. Further, the expression loci of germline proteins (10B) with respect to the position of nuclei can be identified. The distinct structure of the germline cytoskeleton (10C) at the different regions of the germline can be identified.

Box 1.Specific parameters used for imaging. **(A)** Image acquisition parameters for confocal microscopy. **(B)** 3D rendering parameters for each region of the germline. Diameter values are used for developing DAPI stained nuclei and surface detail is used for developing protein distribution. Chromosomes in oocytes were detected and developed based on size and size depends on the separation between chr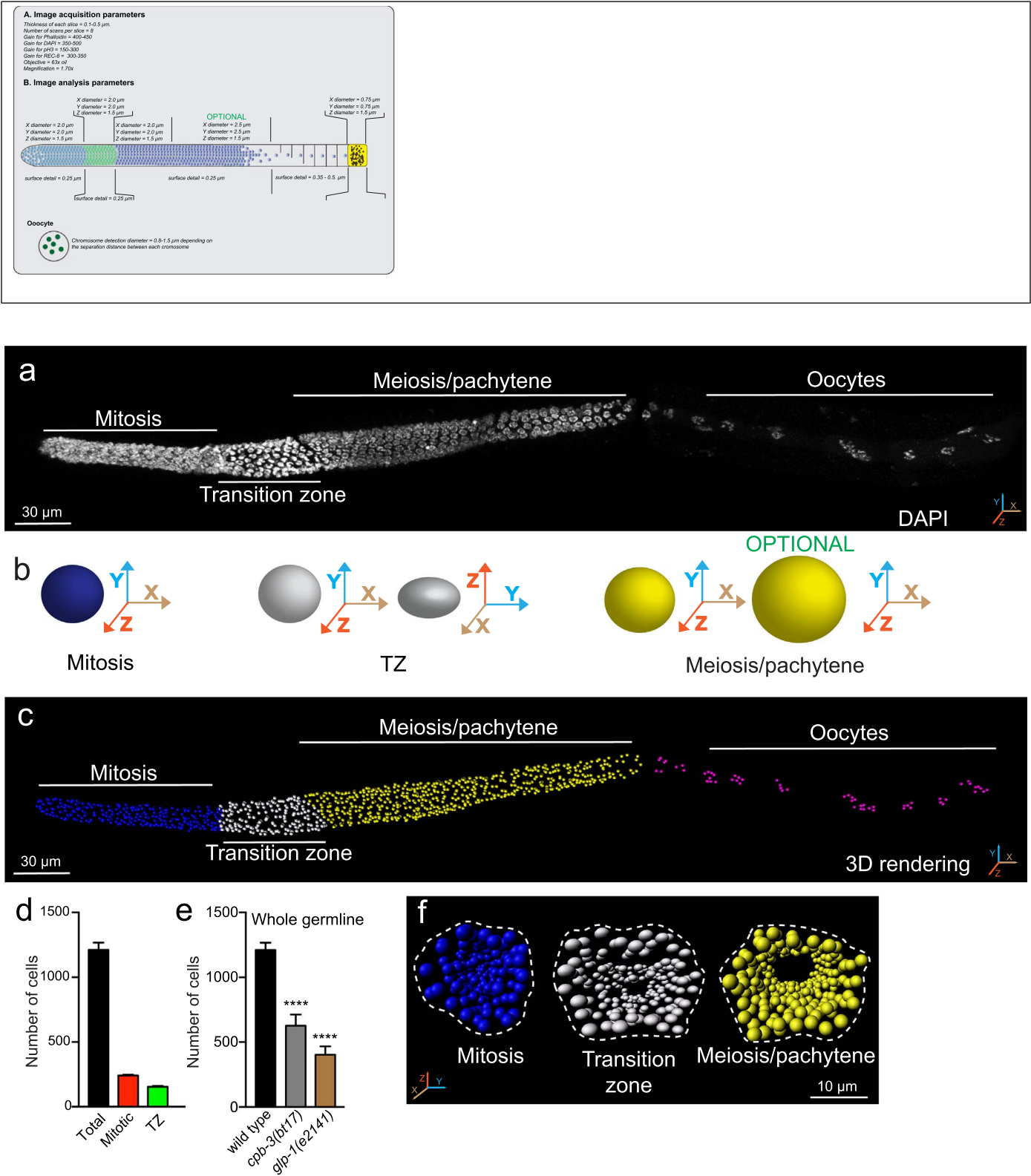omosomes. Download high resolution figure from https://www.sciencedirect.com/science/article/pii/S0012160617306176?via%3Dihub.

Fig. 2. 3D rendering and automated scoring of the germline (a) DAPI stained image of one hermaphrodite germline arm showing the mitotic region, transition zone, meiotic/pachytene region and oocytes. (b) 3D rendering of size and shape for each germline nucleus and the axis of view. See Box 1 for defined parameters. (c) The 3D-rendering of germline nuclear distribution. (d) Automated counting of nuclei in each region of wild type germlines (n=15). (e) Automated counting of total germline nuclei in wild type, *cpb-3(bt17)* and *glp-1(e2141)* mutants (n=10). **** p < 0.0001, *t*-test. (f) YZ axis view showing distinct patterns of nuclear distribution in each germline region. Note - oval-shaped transition zone nuclei (gray) compared to circular mitotic (blue) and meiotic nuclei (yellow).

240–250 nuclei and transition zone = 170–180 nuclei) closely resembles previously published manual counting (Fig. 2**d**) (Eckmann et al., 2004; Kimble and White, 1981). To further establish the accuracy and applicability of this method, we performed analysis of genetic mutants with known germline defects. *cpb-3* encodes a CPEB ortholog that inhibits physiological apoptosis in the germline, and *glp-1* encodes a Notch receptor expressed in the distal end of the germline that promotes mitotic proliferation (Austin and Kimble, 1987; Boag et al., 2005). The absence of both *cpb-3* and *glp-1* cause a significant reduction in germline nuclei number (Austin and Kimble, 1987; Hasegawa et al., 2006). Using automated counting, we confirmed the reported reduction of germ cells in *cpb-3* and *glp-1* mutant germlines (Fig. 2**e and** Supplementary Figure 1c-d), validating the reliability of the method.

Having successfully shown the utility of our method for automated analysis of germline cell counting, we analyzed the nuclear and cytoskeletal organization of 3D-rendered germlines. Analysis of the XYZ organization shows a distinct region-specific pattern of germline nuclear distribution (Fig. 2**f**). By applying specific parameters (refer to Box 1), we found that nuclei in the mitotic region are tightly packed throughout the germline (Fig. 2**f**). As imaging progressed proximally, nuclei reorganize toward the outer edge of the germline, leaving fewer nuclei in the center (Fig. 2**f**). Circumferential redistribution is more distinct in the late meiotic region (Fig. 2**f**). Using an X and Z axis projection, it is possible to quantify the nuclear distribution in each zone. We first selected a two-cell diameter area in the mitotic and pachytene regions of the germline. The selected regions were at a distance of 10-nuclear diameters away from either end of the transition zone. We created boxplots for the axis projection for cells at each region, showing the position of cells in the X and Z axis projection (Supplementary Fig. 1) for an individual germline. Quantification of nuclear distribution in each zone (Supplementary Fig. 1b) shows that the interior of the proximal meiotic germline is less occupied than the distal mitotic region. This analysis suggests that structural differences are present in the germline that may result in such nuclear organization.

To further assess the 3D structure of the germline we analyzed the actin cytoskeleton, which is important for maintenance of germline structural integrity and permits uninhibited cytoplasmic streaming (Wolke et al., 2007). F-actin is an essential structural component of the cytoskeleton and can be stained with phalloidin. 2D analysis shows that germline F-actin is distributed throughout the length of the germline (Fig. 3**a**). Closer examination of the mitotic region shows a distinct 'zigzag' structure of actin close to the DTC in all animals analyzed (Fig. 3**a**).
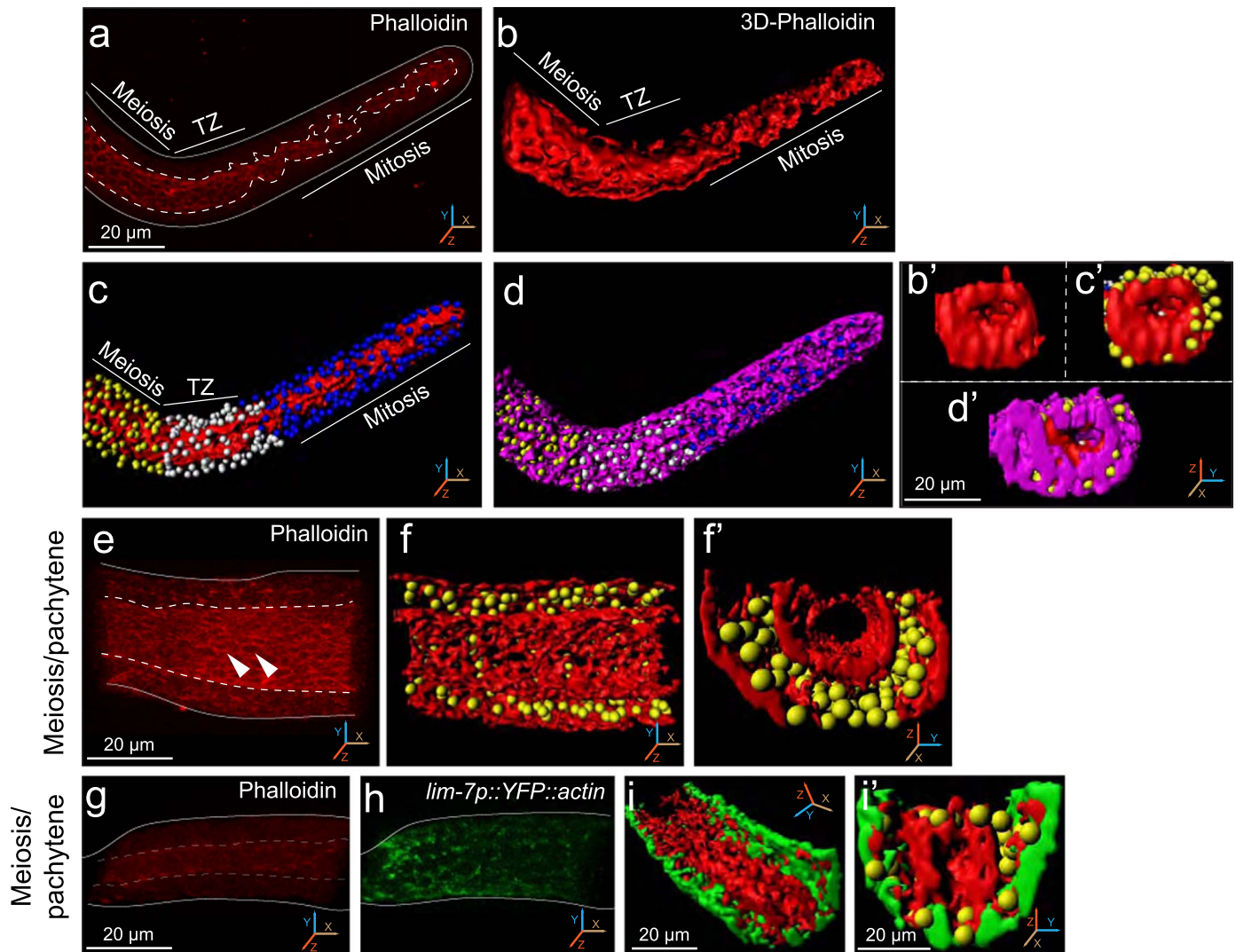

Fig. 3. 3D rendering reveals distinct germline cytoskeletal structures (a) 2D micrograph of F-actin staining of a wild type germline. (b) 3D rendering of the inner cytoskeletal germline tube. (c-d') Germline nuclei (blue, white and yellow) appear embedded in actin clefts on the inner actin tube (red). A second layer of actin (pink) covers the nuclei. (e) 2D micrograph of the late pachytene cytoskeleton. Positions of nuclei are visible (arrowheads). (f-f') Cross-sectional 3D analysis shows distinct actin tubes and nuclear organization. (g-i') 2D micrographs and 3D rendering of F-actin shown by phalloidin staining (red) and YFP-tagged actin expressed on gonadal sheath (green).

To generate a 3D view of the cytoskeleton, phalloidin stained germlines were reconstructed using the surface function of Imaris 8.4.1 software. First, surface detail was defined 0.25 μm for the phalloidin staining. This means that every 0.25 μm will be rendered separately into 3D models before moving to the next point. If more detailed visualization is required, a lower value for surface detail can be selected. For the overall analysis of the mitotic region, transition zone and meiosis region, a surface detail of 0.25 μm is required. However, cytoskeletal analysis at the oocyte region will require a surface detail of 0.35–0.5 μm. This is due to the formation of well-defined fibrous structures and alignment of the cytoskeleton at the oocyte region. With defined surface details, 3D rendering is performed by applying smooth surface development, which creates a complete structure by considering the overall intensity of the staining rather than the intensity at each point. The selection of smooth surface development ensures the uniform development of stained structures. However, more detailed rendering can be obtained by avoiding smooth development. Refer to Box 1 for parameters.

We found that the germline cytoskeleton has two distinct structures establishing a 'tube within a tube' organization (Fig. 3b, d' and Supplementary Movie 1). The difference in intensity of phalloidin staining allows the detection of each structure, even though the tubes maintain contact at some points. The number of contact points is greater towards to distal end of the germline, where the inner cytoskeletal tube appears to be a mass of actin (Fig. 3b and Supplementary Movie 1). Germline nuclei appear embedded in the inner actin structure and are wrapped by an external actin structure (Fig. 3c-d and Supplementary Movie 2). Towards the transition zone, the inner actin assumes a smooth structure (Fig. 3a) and the external actin cytoskeleton, possibly holding the gonadal sheath in position, covers the nuclei and the inner tube (Fig. 3d and Supplementary Movie 3). The YZ view at early meiosis/pachytene shows the 'tube within a tube' structure and nuclear organization in this region (Fig. 3b'-d'). Cross-sectional analysis of late meiosis/pachytene cytoskeleton (20 nuclear diameters away from transition zone) shows two distinct tubes, with the nuclei organized between them (Fig. 3e-f' and Supplementary Movie 4). To confirm these structures are not staining artefacts, we used a *C. elegans* strain where YFP-tagged actin is expressed on the gonadal sheath (*lim-7p::YFP::actin*)

(Kinchen et al., 2005). We applied the same parameters to develop the image for *lim-7p::YFP::actin* worms stained with phalloidin. YFP was detected on the exterior tube co-localizing with phalloidin whereas phalloidin was present on both tubes (Fig. 3i-i' and Supplementary Movie 5). Therefore, our protocol not only demonstrates a reliable method for cytoskeletal studies, but also reveals a potentially physiologically important structure within the germline that may control the distribution of mitotic nuclei and access to proteins in that region. Using a similar protocol, we also examined the cytoskeleton at the oocyte and spermathecal regions, which suggests that oocytes may be housed in regions marked with dense cytoskeleton, as has previously been shown (Fig. 4 and Supplementary Movie 6; Wolke et al., 2007). In addition, our analysis showed the distribution of sperm (Fig. 4a–c) and sperm count (Fig. 4f), which compares well with published data (McMullen et al., 2012).

Supplementary material related to this article can be found online at http://dx.doi.org/10.1016/j.ydbio.2017.10.004.

Analysis of protein expression and distribution is important for deciphering germline phenotypes. A major protein marker that reflects the state of germline nuclei is phosphorylated histone H3 (pH3), which is detected during mitosis and is used to calculate a mitotic proliferation index (Hendzel et al., 1997). pH3 can initiate at different phases of cell division in different organisms, but metaphase chromosomes are always found to be heavily phosphorylated (Rossetto et al., 2012). Germline pH3 staining is routinely assessed manually, however, this has two disadvantages. First, the data only provides the number of histone positive nuclei without accounting for intensity on each chromosome. Second, it can overlook weakly phosphorylated nuclei. Here, with automated rendering, we performed not only counting of pH3 positive nuclei but also identified multiple intensity centers of phosphorylation within each nucleus, suggesting staining of chromosomes. pH3 co-localizes with DAPI staining as shown in Fig. 5a. We defined the size of DAPI stained nuclei in the mitotic region, as detailed above, to render into 3D models. Next, to count the number of pH3 positive nuclei, we defined the XY diameter of pH3 staining to 2.5 μm (Fig. 5b). To identify intensity centers within nucleoli we defined the size of the spots to 0.25 μm on the XY axis. After rendering the 0.25 μm spots to 3D, we generated a heat map where each spot is colored according to the intensity of pH3 staining (Fig. 5c). Our analysis
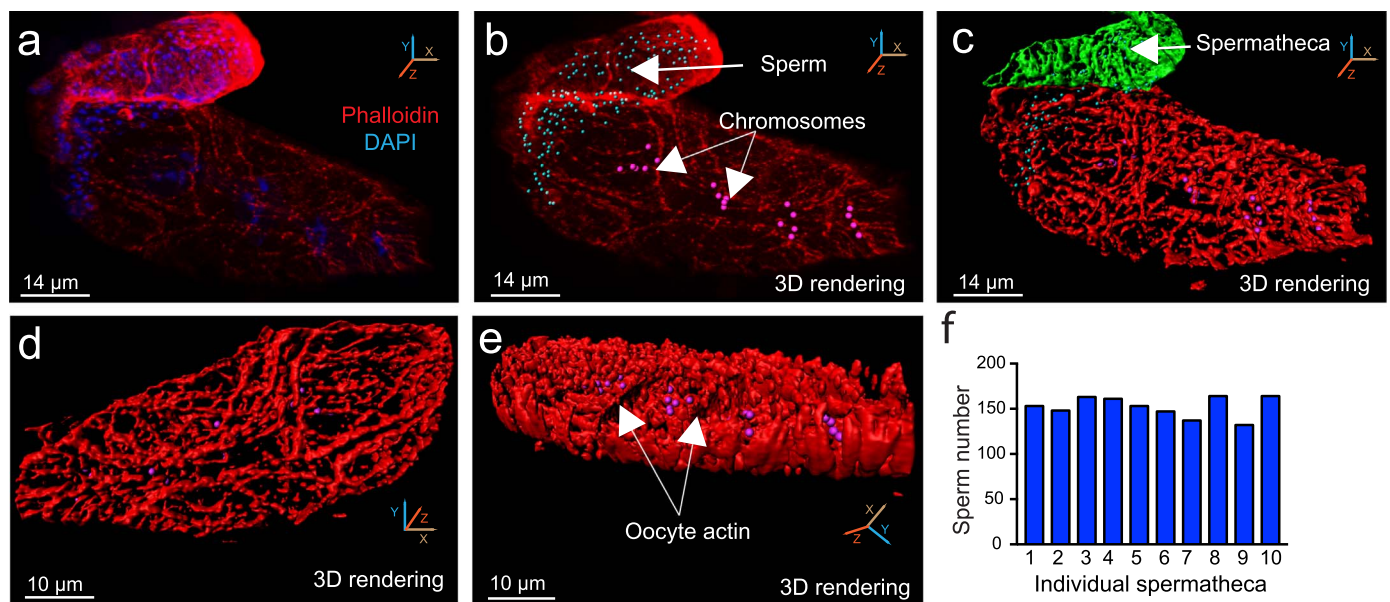

Fig. 4. Cytoskeletal structure at the proximal region of the germline (a) 2D micrographs showing DAPI (blue) and phalloidin (red) staining of the oocyte region and spermatheca. (b) 3D rendering of DAPI staining showing chromosomes in oocytes (pink) and sperm (blue). (c) 3D rendering of the cytoskeleton at oocyte region and spermatheca. The oocyte region appears to be have distinct actin fibers whereas the spermatheca has condensed actin. (d-e) 3D image of the oocyte region showing that the cytoskeleton forms thick fibres of actin and forms cytoskeletal ridges between oocytes (arrows in e). (f) Number of sperm in 12 individual spermatheca of young adult wild type worms. For all images, note the viewing axis shown.
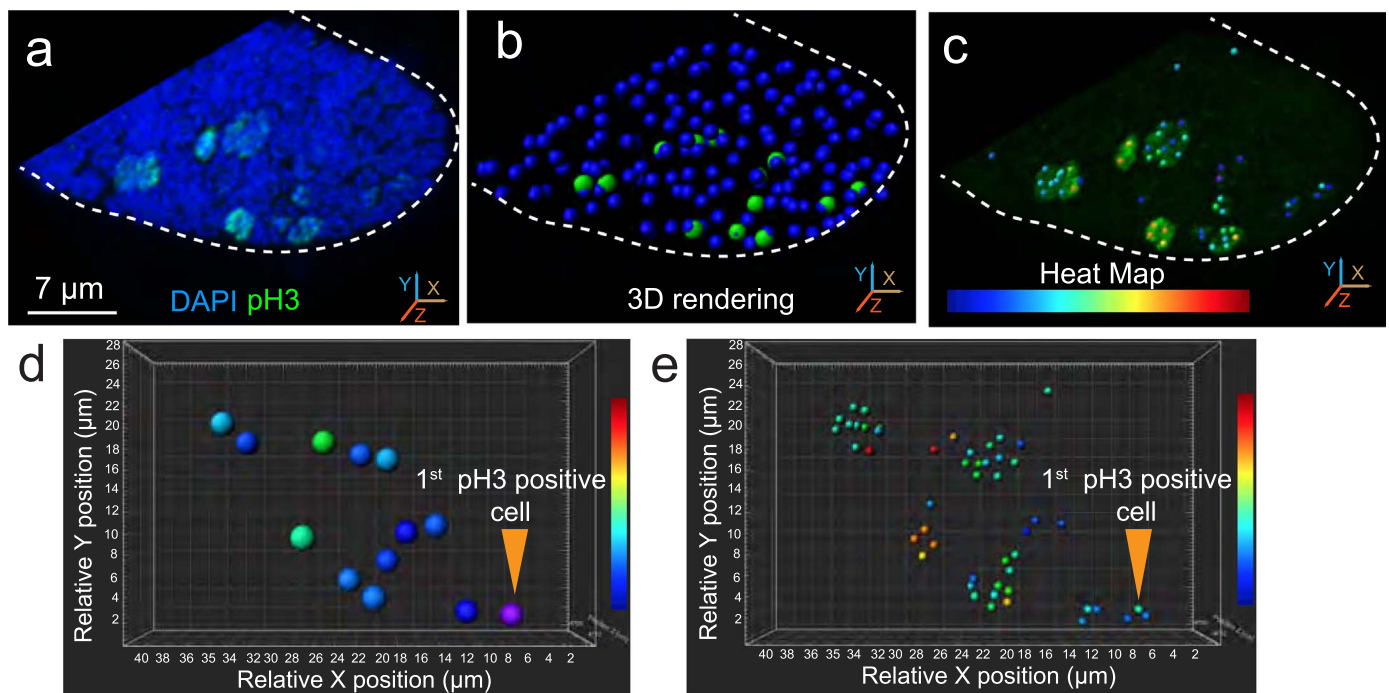
Fig. 5. Imaging and rendering of phosphorylated Histone H3 (pH3) (a) 2D micrograph showing staining for DAPI (blue) and pH3 (green) at the distal end of the germline. (b) 3D rendering of DAPI (blue) and pH3 expressing nuclei (green). (c) Expression heat map of pH3 intensity within each nucleus (red-high, blue-low expression), indicating the stage of chromosome replication. (d-e) 3D graphs showing the relative distance from the distal end to phosphorylated nuclei. Phosphorylation intensity for whole nuclei (d) and intensity centers within each nucleus (e) are shown.

revealed multiple intensity points within each nucleolus, most likely from distinct chromosomes. Using the heap map and relative positioning of nuclei (Fig. 5**d–e**), we show that nuclei close to the DTC have less intense pH3 compared to more proximal nuclei and as nuclei approach the transition zone the pH3 decreases again. As the metaphase chromosomes are heavily phosphorylated for pH3, this analysis can further help to characterize the dynamics of germline cell division. We speculate that this analysis may be used in tandem with staining for other nuclear division and chromosomal markers to predict nuclear division kinetics. Finally, we performed immunostaining for REC-8 protein, which distributes throughout the mitotic region, (Supplementary Fig. 2). As previously published, we found that *glp-1(e2141)* mutant germlines have a decreased proliferative zone size that is concentrated more distally when compared to wild type (Austin and Kimble, 1987).

Taken together, our method overcomes the current limitations of 2D germline analysis, extends previous semi-automated methods (Korta et al., 2012), and provides an efficient and time-saving means of studying nuclear and cytoskeletal organization in the *C. elegans* germline. While we used the protocol to investigate the germline of young adults, the method can be used for 3D rendering of other worm structures (e.g. neurons expressing GFP), 3D analysis of sedated live worms, and analysis of protein distribution in any given structure. Finally, the distinct structural features of the germline revealed here identify a previously unappreciated level of complexity that will inform subsequent studies of the *C. elegans* germline.

3. Materials and methods

3.1. Strains

Wild type (N2, Bristol), *cpb-3(bt17) I, glp-1 (e2141) III* and *opIs110 [lim-7p::YFP::actin + unc-119(+)] IV.*

3.2. Synchronization of worms

For germline phenotypic analysis, worms must be synchronized to enable faithful comparison of phenotypes. To synchronize the worms, we placed 5–6 gravid adult hermaphrodites into the 100 µl bleach solution followed by incubation at 20 °C overnight to allow hatching into L1 larvae. After 48 hrs, L4 larvae can be picked onto new plates and incubated for 16 h at 20 °C until the larvae mature into young adults.

3.3. Staining and confocal microscopy of the C. elegans germline

Sedated young adult hermaphrodites are dissected using needles to isolate the germlines from the worm body and placed on a poly-L-lysine coated slide. The slide containing the dissected worms are fully submerged in liquid nitrogen and then transferred to ice-cold methanol. After 1 min incubation in methanol, worms are fixed in 3.7% PFA in PBS. After washing in PBS-tween-20 and blocking in 5% BSA the germlines are incubated with the primary antibody followed by secondary antibody, DAPI and phalloidin. Confocal imaging can be performed on 0.1–0.5 µm thick slices. Refer to Box 1 for acquisition parameters.

3.4. Generation of 3D germline cytoskeleton images

To generate a 3D view of the germline cytoskeleton, we first used the surface function of the Imaris software. Phalloidin stained germlines were reconstructed using the surface function of Imaris 8.4.1. First, surface detail was defined at 0.25 µm for phalloidin staining. This means that every 0.25 µm will be rendered separately into 3D models before moving to the next point. If more detailed visualization is required, a lower value for surface detail can be selected. For overall analysis of the mitotic region, transition zone and meiotic region, a surface detail of 0.25 µm is required. However, cytoskeletal analysis at the oocyte region requires a surface detail of 0.35–0.5 µm. This is due to the formation of well-defined fibrous cytoskeletal structures at the

oocyte region. With defined surface details, 3D rendering will be performed by applying smooth surface development, which creates a complete structure by considering the overall intensity of the staining rather than the intensity at each point. The selection of smooth surface development ensures the uniform development of stained structures. However, more detailed rendering can be obtained by avoiding smooth development. Refer to Box 1 for parameters.

Additional materials, methods and detailed protocols are available in the online version of the paper.

Acknowledgments

Author Contributions

S.G. and R.P. conceived the project. S.G. performed the experiments. S.G. and R.P. analysed the data and wrote the paper. P.B. contributed reagents, provided advice and provided comments on the manuscript.Competing Financial Interests

The authors declare no competing financial interests.

Appendix A. Supporting information

Supplementary data associated with this article can be found in the online version at doi:10.1016/j.ydbio.2017.10.004.

References

Austin, J., Kimble, J., 1987. glp-1 is required in the germ line for regulation of the decision between mitosis and meiosis in C. elegans. Cell 51, 589–599.

Berry, L.W., Westlund, B., Schedl, T., 1997. Germ-line tumor formation caused by activation of glp-1, a Caenorhabditis elegans member of the Notch family of receptors. Development 124, 925–936.

Boag, P.R., Nakamura, A., Blackwell, T.K., 2005. A conserved RNA-protein complex component involved in physiological germline apoptosis regulation in C. elegans. Development 132, 4975–4986.

Byrd, D.T., Knobel, K., Affeldt, K., Crittenden, S.L., Kimble, J., 2014. A DTC niche plexus surrounds the germline stem cell pool in Caenorhabditis elegans. PLoS One 9, e88372.

Eckmann, C.R., Crittenden, S.L., Suh, N., Kimble, J., 2004. GLD-3 and control of the mitosis/meiosis decision in the germline of Caenorhabditis elegans. Genetics 168, 147–160.

Hasegawa, E., Karashima, T., Sumiyoshi, E., Yamamoto, M., 2006. C. elegans CPB-3 interacts with DAZ-1 and functions in multiple steps of germline development. Dev. Biol. 295, 689–699.

Hendzel, M.J., Wei, Y., Mancini, M.A., Van Hooser, A., Ranalli, T., Brinkley, B.R., Bazett-Jones, D.P., Allis, C.D., 1997. Mitosis-specific phosphorylation of histone H3 initiates primarily within pericentromeric heterochromatin during G2 and spreads in an ordered fashion coincident with mitotic chromosome condensation. Chromosoma 106, 348–360.

Hirsh, D., Oppenheim, D., Klass, M., 1976. Development of the reproductive system of Caenorhabditis elegans. Dev. Biol. 49, 200–219.

Hubbard, E.J., 2007. Caenorhabditis elegans germ line: a model for stem cell biology. Dev. Dyn. 236, 3343–3357.

Joshi, P.M., Riddle, M.R., Djabrayan, N.J., Rothman, J.H., 2010. Caenorhabditis elegans as a model for stem cell biology. Dev. Dyn. 239, 1539–1554.

Kershner, A., Crittenden, S.L., Friend, K., Sorensen, E.B., Porter, D.F., Kimble, J., 2013. Germline stem cells and their regulation in the nematode Caenorhabditis elegans. Adv. Exp. Med. Biol. 786, 29–46.

Kimble, J.E., White, J.G., 1981. On the control of germ cell development in Caenorhabditis elegans. Dev. Biol. 81, 208–219.

Kinchen, J.M., Cabello, J., Klingele, D., Wong, K., Feichtinger, R., Schnabel, H., Schnabel, R., Hengartner, M.O., 2005. Two pathways converge at CED-10 to mediate actin rearrangement and corpse removal in C. elegans. Nature 434, 93–99.

Korta, D.Z., Tuck, S., Hubbard, E.J., 2012. S6K links cell fate, cell cycle and nutrient response in C. elegans germline stem/progenitor cells. Development 139, 859–870.

McMullen, P.D., Aprison, E.Z., Winter, P.B., Amaral, L.A., Morimoto, R.I., Ruvinsky, I., 2012. Macro-level modeling of the response of C. elegans reproduction to chronic heat stress. PLoS Comput. Biol. 8, e1002338.

Rossetto, D., Avvakumov, N., Cote, J., 2012. Histone phosphorylation: a chromatin modification involved in diverse nuclear events. Epigenetics 7, 1098–1108.

Salinas, L.S., Maldonado, E., Navarro, R.E., 2006. Stress-induced germ cell apoptosis by a p53 independent pathway in Caenorhabditis elegans. Cell Death Differ. 13, 2129–2139.

Schumacher, B., Hanazawa, M., Lee, M.H., Nayak, S., Volkmann, K., Hofmann, E.R., Hengartner, M., Schedl, T., Gartner, A., 2005. Translational repression of C. elegans p53 by GLD-1 regulates DNA damage-induced apoptosis. Cell 120, 357–368.

Wolke, U., Jezuit, E.A., Priess, J.R., 2007. Actin-dependent cytoplasmic streaming in C. elegans oogenesis. Development 134, 2227–2236.